A novel double perovskite oxide Sm$_2$CoFeO$_6$ phosphor for orange LEDs: structural, magnetic and luminescence properties

M. Dhilip^1 · J. Stella Punitha^2 · R. Rameshkumar^1 · S. Rameshkumar^1 · P. Karuppasamy^1 · Muthu Senthil Pandian^1 · P. Ramasamy^1 · K. Saravana Kumar^3 · V. Anbarasu^4 · K. Elangovan^5

Abstract

Double perovskite Sm$_2$CoFeO$_6$ (SCFO) compound has been synthesized by the conventional solid-state reaction route for the first time. The Rietveld refinement has been carried out using the X-ray diffraction data; it confirms the single-phase formation of orthorhombic structure with the *Pnma* space group. UV-DRS results show that SCFO was observed in semiconducting behavior. Spin–phonon coupling of SCFO was observed from Raman spectroscopy investigation. The Raman analysis and group theory confirms that the IR and Raman active modes of SCFO. The amount of Sm, Co, Fe and O elements in the SCFO compound was examined by energy-dispersive spectroscopy (EDS) with the assistance of field emission scanning electron microscopy (FE-SEM) analysis. The photoluminescence excitation and emission spectra of SCFO were examined. The results show that the phosphor is excited in the region from 320 to 500 nm, and it emits orange at 607 nm, due to the resultant of $^4G_{5/2} \rightarrow {^6H_{7/2}}$ transitions. The SCFO compound exhibited ferromagnetic behavior, which is confirmed by VSM analysis. The obtained results demonstrated that SCFO double perovskite is extensive for application of spintronic devices and LED's.

1 Introduction

Double Perovskites A$_2$BB'O$_6$ (A is a rare earth element; B and B' are transition metals) have a revival of scientific importance due to their prosperous physical properties and potential of technical utilization at room temperature. It also exhibits a variety of properties like electromechanical coupling, nonlinear optical response, photo-catalytic activity and piezoelectricity [1–3]. Hence, it attracts substantial interest in fundamental research and for applications in spintronics, sensor, transducer, actuator and other technological field [4–8].

To address all ambiguities, regularly distributed, identical and single-phase material is needed so that the real mechanism of the A^{3+} dependence of magnetization can be explained. Hence, A$_2$CoFeO$_6$ (ACFO) family was synthesized by the solid-state reaction technique and taking into account the interesting variety of structure, electronic properties and competing magnetic relations in the family, a broad study has been performed to establish the control of the rare earth size on the structural and the magnetic ground states of these compounds. Such a complete study of the ACFO family is a new addition to the ongoing research in the field.

Recently, there has been a resurgence of importance in Cobalt Ferrite materials of vital technological interest due to their abundant physics and potential applications in the preparation of the optoelectronics, microwave frequency devices, storage media and gas sensors [9–12]. Owing to their important magnetic and optical properties, ferrites are extensively

✉ M. Dhilip
  ceramatdhilip@gmail.com

1   SSN Research Centre, Sri Sivasubramaniya Nadar College of Engineering, Chennai, Tamil Nadu 603 110, India

2   Department of Physics, SRM Institute of Science and Technology, Chennai, Tamil Nadu 600 089, India

3   Department of Physics, Sri S. Ramasamy Naidu Memorial College, Sattur, Tamil Nadu 626 203, India

4   Department of Physics (Self-Finance), PSG College of Arts and Science, Coimbatore, Tamil Nadu 641 014, India

5   Department of Physics, Dhanalakshmi Srinivasan Arts and Science (Co-Education) College, Mamallapuram, Chennai, Tamil Nadu 603 104, India

used in the electronic industry. Thermal stability, mechanical hardness, and a large coercive field are all advantages. Many studies on the structural, electrical and magnetic properties of various double perovskite oxides have been published recently. The discovery of Cobalt ferrite-based double perovskites oxides has recently heightened the family's prominence, The coercivity of $SmCoO_3$ has recently been reported to be greater than 30 kOe. It would be fascinating to look into this phase further for spintronic applications [13, 14]. Due to intriguing ferromagnetic properties, $SmFeO_3$ ortho-ferrite has been widely explored for magnetic properties [15, 16]. At the same time, investigations on the magnetic properties of the double perovskite Sm_2CoFeO_6 compound have yet published in the literature. The samarium cobalt ferrites with a chemical formula Sm_2CoFeO_6 related to double perovskite structure ($A_2BB'O_6$) have caused greater attention in recent years for two reasons. First, they are key materials for any high technical applications such as recording devices, sensors, magnetic drug delivery, magnetic cards, catalysis, biomedical, solar cells and biotechnology. Second, they exhibit the features of cobalt ferrites that are intensely charged on a sequence of features such as micro structural characteristics and chemical composition.

Cobalt ferrites containing double perovskites have been advised as potential compounds for magnetic data storage device applications. The lack of work in the literature of the double perovskite SCFO compound [17–22]. So for, we have chosen to investigate magneto-optical properties. The aim of the present study is synthesize, structural, optical and magnetic properties of the double perovskite SCFO compound for the magneto-optical and spintronic applications. The methodology is presented in Sect. 2. The result and discussion and conclusions are presented in Sects. 3 and 4, respectively.

2 Experimental method

2.1 Sample preparation

Commercially available Sm_2O_3 (Alfa Aesar 99.99%), Co_3O_4 (Alfa Aesar 99.99%) and Fe_2O_3 (Alfa Aesar 99.85%) powders were purchased and weighed accurately in required proportions, then mixed thoroughly and ground well with an Agate mortar and pestle to convert very fine powders. The polycrystalline sample of Sm_2CoFeO_6 compound was prepared by the traditional standard solid-state ceramic technique. Then, heated for 24 h in an air environment at 1000 °C with intermediate regrinding. To ensure that the full reaction, efficient, high temperature annealing process is adopted, it is followed by the final sintered at 1100 °C for 48 h with intermediate regrinding and repelling.

2.2 Characterizations

To study the structural phase purity, cell dimensions and uniformity, the powder X-ray diffraction (XRD; X-ray powder SIEMENS diffractometer) at room temperature was employed using Cu-Kα radiation from 20° to 80°. The structural features were obtained by the Rietveld refinement [23]. The Raman spectral analysis was performed with Renishaw Plc. micro-Raman spectrometer with a 514 nm excitation wavelength. The Argon ion laser was used as a source in the extended range of 100—2000 cm^{-1} wavenumber. Diffuse reflectivity spectroscopy (DRS) measurement was used to determine the band gap energy of the produced sample. The test was carried out by UV–VIS–NIR spectrophotometer at the wavelength range of 200 to 800 nm (JASCO V-670). The photoluminescence measurement was performed by using an Argon ion laser (Omni Chrome, Model 532-MAP, USA), excitation source wavelength 465 nm, power of 90 mW, monochromator (SPEX, Model 207, USA) and InGaAs detector (Electro-Optical Systems, Model ILN-030, USA). Scanning electron microscopy (SEM) was used to investigate the microstructure behavior and phase purity of SCFO by utilization of Philips FEI QUANTA 200 field emission equipment with the energy-dispersive spectra (EDS). The magnetic measurements were carried out at room temperature using a Lakeshore VSM 7410S instrument.

3 Results and discussion

3.1 Structural analysis

Single-phase SCFO double perovskite sample was prepared using the conventional solid-state reaction route at 1100 °C without any impurities or secondary phases. The powder XRD data were carried out for SCFO at room temperature. The Rietveld refinement of XRD patterns for SCFO has been presented in Fig. 1a. Figure 1a shows that the black color solid line indicates the observed (experimental) XRD data, whereas the red color dots represent the calculated XRD data. The green color vertical lines represent the difference between the calculated and observed data. The XRD results indicate that SCFO compounds exist in single-phase orthorhombic structure with the *Pnma* space group. The crystal structure of the SCFO with the *Pnma* space group is drawn using Vesta software [24], which is shown in Fig. 1b. The Rietveld refinement optimized crystallographic data are presented in Table 1.

The modified tolerance factor is used to determine the structural perfection and structural stability. The tolerance

Fig. 1 **a** The Rietveld refinement of the room temperature XRD pattern for SCFO compound. **b** The Orthorhombic structure with Pnma space group of SCFO represented on Vesta software program
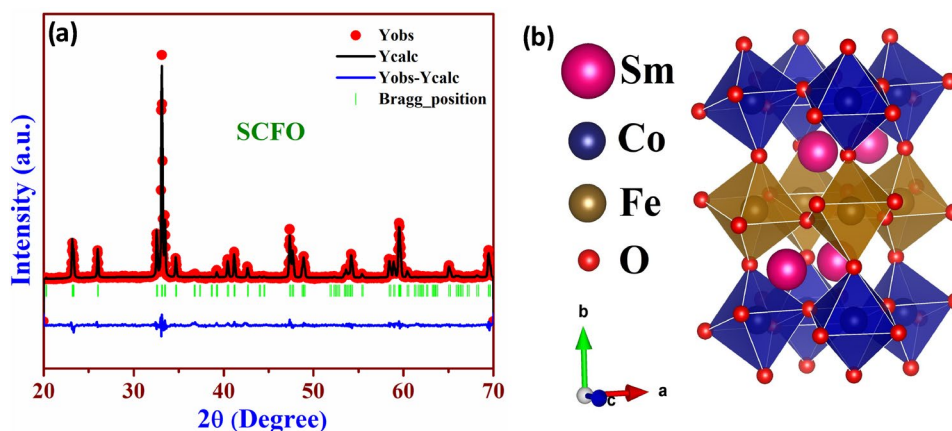
Table 1 **a** Crystallographic data and **b** fractional atomic coordinates for SCFO at room temperature determined by Rietveld refinement of the powder XRD pattern

(a) Crystallographic data

Space group = *Pnma* (62)		
a = 5.4986 Å	V = 224.584 Å^3	Chi^2 = 3.784
b = 7.6254 Å	R_{wp} = 10.7	GOF = 1.9
c = 5.3563 Å	R_{exp} = 5.52	

Atom (site)	X	Y	Z
(b) Fractional atomic coordinates			
Sm (4c)	0.05359	0.25000	0.99090
Co/Fe (4b)	0.000 00	0.000 00	0.50000
O1 (4c)	0.48420	0.25000	0.07986
O2 (8d)	0.70552	0.95177	0.30209

factor (T_f) of Sm$_2$CoFeO$_6$ compound can be stated as in the usual form of double perovskites with mixed A$_2$ BB'O$_6$ [25].

$$\text{Tolerance Factor} \left(T_f\right) = \frac{R_{Sm} + R_O}{\sqrt{2}\left[\frac{R_{Co}+R_{Fe}}{2} + R_O\right]},$$

where R_{sm}, R_{co}, R_{Fe} and R_o are the ionic radii of the corresponding ions. From the literature [25], the tolerance factor (T_f) of the double perovskite characterized into (1) cubic (1.05 > t > 1.00), (2) orthorhombic either monoclinic (t < 0.97) and (3) tetragonal (1.00 > t > 0.97). As our estimated value of T_f for SCFO is less than 0.97, the structure of the compound may be predicted in the orthorhombic crystal system. It is worth noting that based on the ionic radii by calculated T_f of Sm$_2$CoFeO$_6$ is 0.81, i.e., very close to 0.81, which, in turn, is also in good agreement with orthorhombic structure observed as per XRD analysis.

The crystallite size (*D*) of the prepared material has been calculated by using the Scherrer's equation, $D = 0.9\lambda/\beta\cos\theta$), Here, λ is the wavelength, β is the full-width half-maxima (FWHM), and θ is the diffraction angle [26, 27], and it was obtained to be 90 nm.
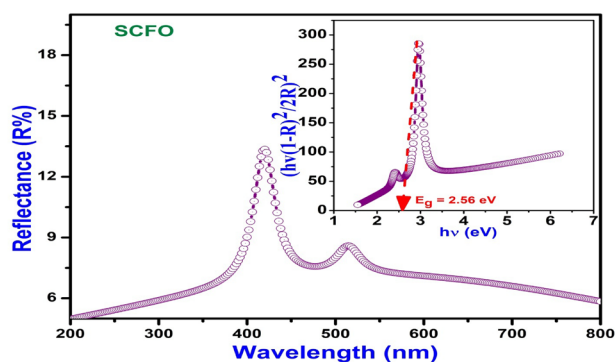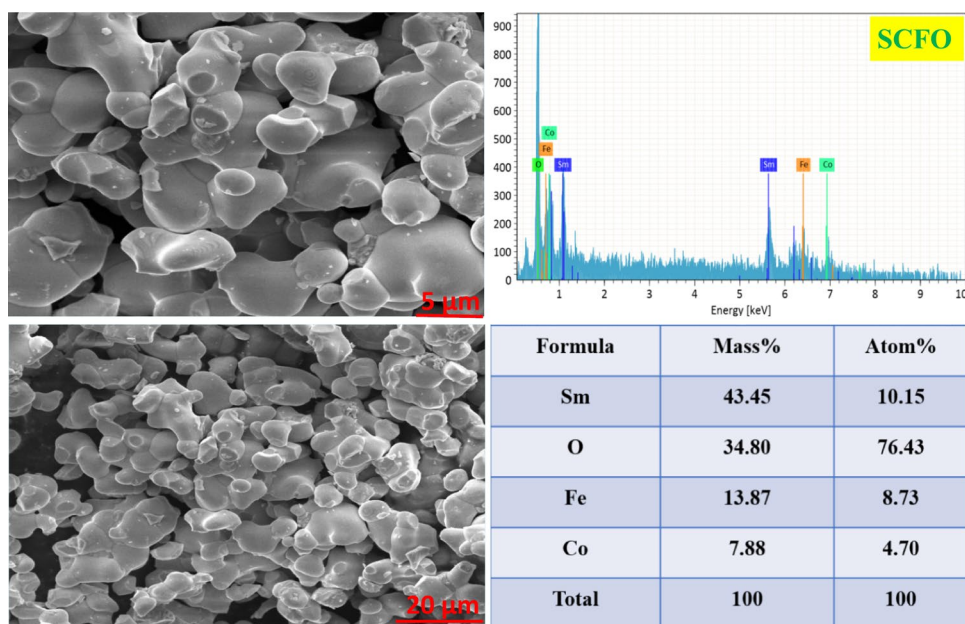
3.2 Scanning electron microscopy (SEM) analysis

Figure 2 shows the scanning electron microscope images of the SCFO sample viewed on the exposed microstructure character. It was observed that the oxide samples were highly dense with no porosity developed as revealed in figure for Sm$_2$CoFeO$_6$ composition. It was clear from the SEM image, so as to the micron scales (5 and 20 μm) were obtained for SCFO compound.

3.3 Energy-dispersive spectroscopy (EDS)

The elemental composition and their proportion of the SCFO have been confirmed by EDS with the assist of SEM image spectra that are shown in Fig. 2. EDS spectra show the peaks of the elements, Sm (43.45%), Co (7.88%), Fe (13.87%), O (34.80%), and there is no impurity peak in it

Fig. 2 Scanning electron micrographs at various magnifications (5 μm and 20 μm) and Energy Dispersive Spectra for SCFO compound

Formula	Mass%	Atom%
Sm	43.45	10.15
O	34.80	76.43
Fe	13.87	8.73
Co	7.88	4.70
Total	100	100

Fig. 3 UV-DRS Spectra of SCFO. Inset shows Kubelk Munk Plot

which is the evidence of pattern pure phase of SCFO in the atomic concentrations.

3.4 UV-diffuse reflectance spectroscopy (DRS)

The optical properties of SCFO were determined using UV–Vis DRS spectroscopy, which is presented in Fig. 3. It shows the diffuse reflectance spectrum (DRS) of the SCFO compound at room temperature in the range of 200–800 nm. The strong absorption edge near 420 nm (eV) relates to p–d charge transfer transition [O (2p)→Co/Fe (3d)] in the octahedral centers in SCFO.

The absorption coefficient can be performed for the SCFO compound from the diffuse reflectance data using the Kubelka–Munk (KM) function [28, 29]

$$F(R\alpha) = \frac{\alpha}{S} = \frac{(1 - R\alpha)^2}{2R\alpha},$$

where $F(R\alpha)$ represents the KM function, α shows the absorption coefficient, S performs the scattering coefficient, and R represents the reflection coefficient. The band gap energy (E_g) of these compounds was projected from the graph of the square root of the Kubelka–Munk function (hυ$(1-R)^2/2R^2$) versus photon energy (hυ(eV)) as shown in inset Figure. The obtained result of UV–Vis diffuse reflectance (UV-DRS) and the optical band gap energy ($E_g = 2.56$ eV) of the compound indicate that they can be ordered as a semiconductor compound.

3.5 Micro-Raman spectroscopy

Raman spectroscopy is a powerful probe to observe the crystal structure, spin-phonon coupling, cation disorder, impurity phases and dynamical/local lattice distortion present in the materials [30]. The distortions from orthorhombic *pnma* lattice (D^{16}_{2h}) result in SCFO ordered double perovskites. The vibrational modes arise from the (Co/Fe)O$_6$ octahedra and Sm–O bonds. The Raman spectra of the SCFO sample were calculated with excitation wavelength 514 nm that is presented in Fig. 4. The vibrational modes of the synthesized samples were investigated in order to recognize the non-radiative relaxation. Raman spectral study was used to expect the vibrational phonon modes of SCFO in the range 100–2000 cm^{-1}. According to group theory analysis [30,
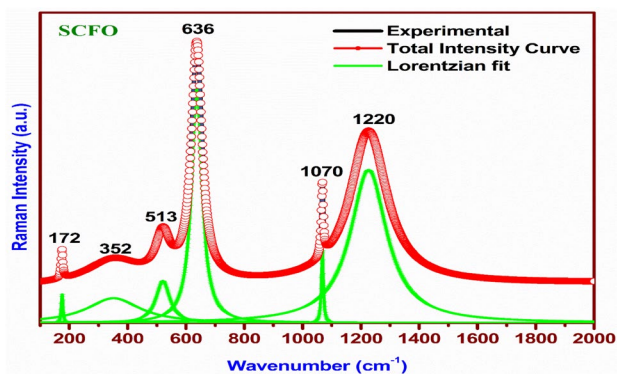
Fig. 4 Raman active region of SCFO compound (The Black lines are experimental data, the strong curves with green shade are the fitting of Lorentzian shapes, and the solid curves with red shade are the total intensities of the Lorentzian lines)

31], the following modes assigned as the SCFO compound is crystallized in primitive orthorhombic structure with the *Pnma* space group, and its point group is D_{2h} (mmm). The SCFO compound is 10 atoms per primitive cell and two formula ($Z=2$) per unit cell, So for 20 atoms per unit cell. Each atom has three degrees of freedom, so it has 60 normal modes of vibrations.

The total mechanical irreducible representation is,

$$\Gamma_{total} = 7A_g + 8A_u + 5B_{1g} + 10B_{1u} + 7B_{2g} + 8B_{2u} + 5B_{3g} + 10B_{3u},$$

$$\Gamma_{accoustic} = B_{1u} + B_{2u} + B_{3u},$$

$$\Gamma_{optical} = 7A_g + 8A_u + 5B_{1g} + 9B_{1u} + 7B_{2g} + 7B_{2u} + 5B_{3g} + 9B_{3u}.$$

The irreducible representation of each atomic contribution, site symmetry, Wyckoff position, IR and Raman active modes are presented in Table 2. Among all of 60 modes of vibrations, there are 25 IR active modes ($9B_{1u} + 7B_{2u} + 9B_{3u}$), 24 Raman active modes ($7A_g + 5B_{1g} + 7B_{2g} + 5B_{3g}$) and 8 Au modes are silent [32, 33].

The Raman spectrum with a fitted Lorentzian curve of SCFO compound is presented in Fig. 4. From the figure observed, the presence of Raman active mode of the SCFO compound is given in Table 3. It shows that the Raman active modes of SCFO are 172, 352, 513, 636, 1070 and 1220 cm^{-1}. These resultant modes are consistent with available references [34, 35]. There are two strong Raman active modes exhibited at 636 cm^{-1} and 1220 cm^{-1}. The strong mode of 636 cm^{-1} (Lower frequency) is attributed to the B_{3g} mode, while the remaining mode at 1220 cm^{-1} (Higher frequency) is allocated to the $2B_{2g}$ mode.

The first order phonon (lower frequency) Raman modes were assigned to the A–O bonds, while the second order phonon (higher frequency) Raman modes were attributed to the B–O bonds. A recommendation can be formed into first order mode peaking around the range of 900–2000 cm^{-1}, almost the higher order frequency values of A$_g$, and B$_g$

Table 2 The irreducible representation of each atomic contribution, site symmetry, Wyckoff position, IR and Raman active modes

Atom	Wyckoff position	Site symmetry	Atomic coordinates			Irreducible representations	Raman active	IR active
			X	Y	Z			
Sm	4c	C_s	0.0535	0.2500	0.9909	$2A_g + A_u + B_{1g} + 2B_{1u} + 2B_{2g} + B_{2u} + B_{3g} + 2B_{3u}$	$A_g, B_{1g}, B_{2g}, B_{3g}$	B_{1u}, B_{2u}, B_{3u}
Fe(Co)	4b	C_i	0.0000 (0.0000)	0.0000 (0.5000)	0.5000 (0.5000)	$3A_u + 3B_{1u} + 3B_{2u} + 3B_{3u}$	None	B_{1u}, B_{2u}, B_{3u}
O1	4c	C_s	0.4841	0.2500	0.0798	$2A_g + A_u + B_{1g} + 2B_{1u} + 2B_{2g} + B_{2u} + B_{3g} + 2B_{3u}$	$A_g, B_{1g}, B_{2g}, B_{3g}$	B_{1u}, B_{2u}, B_{3u}
O2	8d	C_1	0.7055	0.9517	0.3020	$3A_g + 3A_u + 3B_{1g} + 3B_{1u} + B_{2g} + 3B_{2u} + 3B_{3g} + 3B_{3u}$	$A_g, B_{1g}, B_{2g}, B_{3g}$	B_{1u}, B_{2u}, B_{3u}

Table 3 Symmetry assignments of Raman active modes for the observed peaks

Raman shift (cm^{-1})		Assignment of modes
Experimental	References [30, 33]	
172	172	B_{2g}
352	352	B_{1g}
513	513	B_{2g}
636	637	B_{3g}
1070	(The stretching vibration modes in Co–O–Fe sub-lattices are attributed to the modes observed at 1070 and 1220 cm^{-1})	$2B_{1g}$ Present work. (See text)
1220		$2B_{2g}$ Present work. (See text)

(above 900 cm^{-1}) normal modes present in SCFO, based on the case of the broad higher order frequency modes. It is the displacement of oxygen atoms along the B–O axis with B–O bonding forces and distance influencing its frequency the most [36, 37].

The second order phonon Raman scattering was associated with two strong wide modes found near 1070 and 1220 cm^{-1} [32, 33]. Because it contains phonons across the whole Brillouin-zone, it also contains the frequencies of detected second order phonons at the Γ-point. The two strong second order modes identified between 1070 and 1220 cm^{-1} are slightly asymmetric, as seen in the figure and may be characterized using Chandramohan's [38] approach in the following way, first way to begin with the Co and Fe sites may not be totally ordered, and the altered Co/Fe–O stretching vibrations are close in frequency, allowing the band envelope to contain the uncertain contributions from distinct CoO_6 and FeO_6 environments. Second, domains with varying degrees of Co and Fe order will contribute to the Co/Fe–O stretching bonds in different ways. Finally, the movement of oxygen atoms along the B–O axis corresponds to the second order frequency Raman active modes A_g and B_g, and their frequency is primarily influenced by bonding forces and B–O distance [39, 40].

3.6 Photoluminescence

The excitation spectra of SCFO phosphor recorded at 607 nm emission are shown in Fig. 5. SCFO phosphor features a broad band in the UV region, centered at about 402 nm, with many sharp lines in its excitation spectra between 320 and 420 nm. The excitation range of 320–420 nm is sufficient to ensemble the needs of UV LED's [41]. The most powerful peak at 402 nm appears to show that the excitation spectrum is divided into two portions, as shown in Fig. 5. (1) Due to the samarium-oxygen interactions, the broad absorption band between 320 and 500 nm is known as the charge transfer state (CTS) band. An electron transfer from an oxygen 2p orbital to an empty 4f shell of samarium causes the strongest excitation peak, which is about 402 nm. (2) The Sm^{3+} f–f transition is responsible for a sequence of sharp lines ranging from 320 to 420 nm. Phosphor can absorb the energy of natural light efficiently and completely due to its broad excitation band.

The strongest sharp peak occurs at 402 nm, which corresponds to the Sm^{3+} is $^6H_{5/2} \rightarrow {}^6P_{3/2}$ transition. Other broad excitation peaks at 331 and 346 nm are associated with intra configurationally 4f—4f transitions of Sm^{3+} ions in host lattices, which are assigned to $^6H_{5/2} \rightarrow {}^4P_{3/2}$ and $^6H_{5/2} \rightarrow {}^4D_{7/2}$ transitions, respectively [42]. Near UV (NUV) at about 402 nm can successfully excite the produced SCFO Phosphor [43]. As a result, it works well with UV and NUV-LED, indicating that it has a lot of practical uses [44].

SCFO phosphor emission spectra were measured in the 550–750 nm region. The resulting phosphor's emission spectrum consisted of a series of hard emission lines when excited at 401 nm. Three observed emission peaks in the SCFO emission profile (Fig. 5) correspond to distinctive emission transitions from the excited states $^4G_{5/2}$ to the ground state $^6H_{j/6}$ ($j = 5, 7, 9$) [45–47]. The magnetic dipole transition is represented by the yellow emission at roughly 579 nm is $^4G_{5/2} \rightarrow {}^6H_{5/2}$ transition, while the mixed magnetic-electric dipole $^4G_{5/2} \rightarrow {}^6H_{7/2}$ transition of Sm^{3+} is represented by the orange emission at 607 nm. The transition rarely fluctuates with the crystal field intensity. The red emission at 659 nm is due to Sm^{3+} electric dipole

Fig. 5 Photoluminescence emission spectra of SCFO compound. Inset shows excitation Spectra
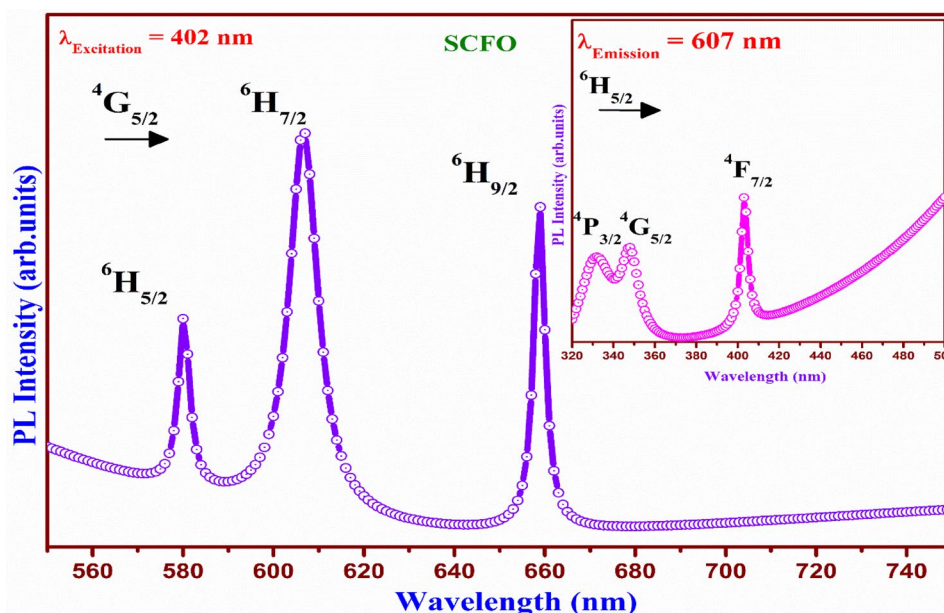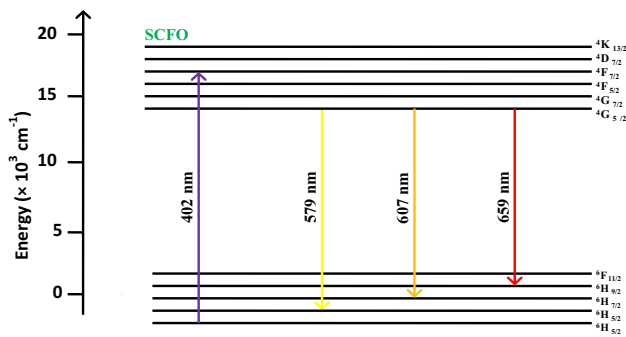
Fig. 6 Energy level diagram and emission transitions of SCFO compound
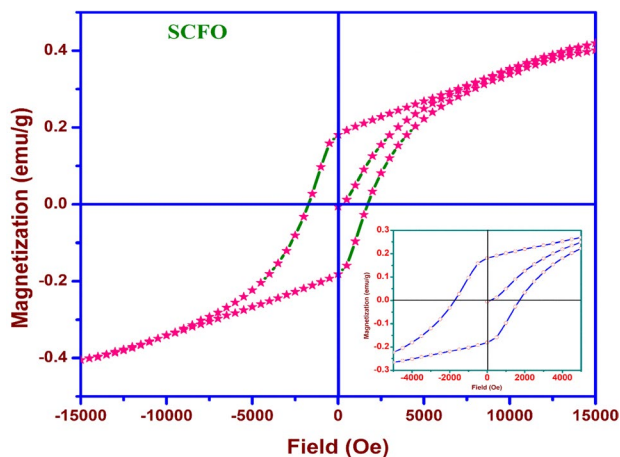
Fig. 7 Room-temperature magnetization curves obtained for SCFO compound. (Inset: Partially enlarged view of M vs H)

$^4G_{5/2} \rightarrow {}^6H_{9/2}$ transition, which is extremely sensitive to the surrounding environment and is determined by the crystal field's symmetry [48, 49]. Inset Fig. 5 shows the results of monitoring the excitation at 402 nm in solid state at room temperature. The strongest orange emission peak will be dominated for the SCFO phosphor developed in our work, which is positioned at 607 nm. The inversion symmetric center in the host lattice is thought to be occupied by Sm^{3+} ions. Figure 6 shows a schematic energy level diagram of SCFO phosphors with different emission bands.

3.7 Magnetic properties

An M–H investigation was carried out at room temperature to explore the magnetic characteristics of SCFO compounds, as shown in Fig. 7. This is done with a magnetic field of −15 to +15 kOe applied. The examined compound showed a hysteresis, which was attributed to ferromagnetic (FM)

activity [50]. The material was designed to have hysteresis, with a residual magnetization value of 0.018124 emu/g and a coercive field value of 1726.8 Oe. The saturation of magnetic moment/mass was calculated to be 0.04124 emu/g. Magnetic hysteresis in combination with non-zero values of magnetic properties (retentivity and coercivity) suggests ferromagnetic behavior [51, 52]. The magnified regions around the origin (inset in Fig. 7) shows that the coercivity is more obvious.

The saturation magnetization is found possible in the Sm$_2$CoFeO$_6$ compound due to fact that of parallel spin alignment of Sm^{3+}, Co^{3+} and Fe^{3+} ions in the crystal symmetry of Sm$_2$CoFeO$_6$ compound. At room temperature, the alternate alignment of SmCoO$_3$ and SmFeO$_3$ sub-lattices formulate the magnetic structure of the material. This complex magnetic ordering exist in the material competes with each other and leads to ferromagnetic ordering. Hence, the anti-phase interface between two areas and/or antisite faults may cause FM interactions. FM interaction between (Co, Fe) and Sm ions located at two separate locations on the A$_2$B'B''O$_6$ perovskite structure may explain this result. This cobaltite behavior can be explained using either a super-exchange (SE) or a double-exchange (DE) mechanism. However, if the ferromagnetism of the stoichiometric perovskite Sm$_2$CoFeO$_6$ can be characterized by the presence of ferromagnet SE Co^{3+}–O–Co^{4+} contacts, the Goodenough-Kanamori rule can be applied. Antiferromagnetic Co^{3+}–O–Co^{3+} (SE) interactions should be detected as well, but this is not the case. In Sm$_2$CoFeO$_6$, the Fe and Co cations have mixed valence states of $3+/4+$ and $3+/4+$, respectively. The mixed valency and random crystallographic occupancy set the setting for ferromagnetic interactions among the transition metal cations, resulting in inhomogeneous magnetic behavior in Sm$_2$CoFeO$_6$. The magnetic exchange in a fully ordered double perovskite is dominated by the ferromagnetic Fe^{3+}–O–Co^{4+}. Electronic transfer from Fe^{3+} high spin state ($S = 5/2$) to Co^{4+} low spin state ($S = 1/2$) can be facilitated via Fe–O–Co exchange pathways[53]. Ferromagnetism in the related system is described within an exchange mechanism model by Pradheesh et Al. [54] and Samia Ben Hammouda et al. [55]. As a result, the DE mechanism, which was earlier proposed for perovskites based on Lanthanum cobaltite, has been confirmed [56, 57].

4 Conclusions

In the present work, double perovskite oxide SCFO compound was synthesized by the solid-state reaction technique. The crystal structure of SCFO was found to be orthorhombic with *Pnma* space group. UV-DRS result observed that SCFO exhibit in semiconductor nature. The

occurrence of first and second order Raman's modes in the deconvolution of Raman's spectra of SCFO compound offers structural evidence. UV radiation in the range of 320–420 nm has activated the phosphor and the transition from $^4G_{5/2}$ to $^6H_{7/2}$ results in an orange emission at 607 nm. Broad bands in the excitation photoluminescence spectra between 320 and 410 nm were linked to the charge transfer band of SCFO. The magnetic property revealed that the SCFO was exhibit in ferromagnetic behavior, so this compound is useful in the fields of solid state lasers, orange LEDs and spintronic applications.

Declarations

Conflict of interest All the authors of this manuscript declare that there has been no more conflict of interest.

References

1. M. Lezaic, N.A. Spaldin, High-temperature multiferroicity and strong magnetocrystalline anisotropy in 3d–5d double perovskites. Phys. Rev. B Condens. Matter Mater. Phys. **83**, 024410 (2011)

2. T.Y. Cai, S.C. Liu, S. Ju, C.Y. Liu, G.Y. Guo, Multiferroic double perovskites $ScFe_{1-x}Cr_xO_3$ ($1/6 \leq x \leq 5/6$) for highly efficient photovoltaics and spintronics. Phys. Rev. Appl. **8**, 1 (2017)

3. Y. Tokunaga, S. Iguchi, T. Arima, Y. Tokura, Magnetic-field-induced ferroelectric state in $DyFeO_3$. Phys. Rev. Lett. **101**, 3 (2008)

4. M. Dhilip, N. AparnaDevi, J. StellaPunitha, V. Anbarasu, K. SaravanaKumar, Conventional synthesis and characterization of cubically ordered La_2FeMnO_6 double perovskite compound. Vacuum **167**, 16 (2019)

5. Y. Tokunaga, N. Furukawa, H. Sakai, Y. Taguchi, T.H. Arima, Y. Tokura, Composite domain walls in a multiferroic perovskite ferrite. Nat. Mater. **8**, 558 (2009)

6. R. Ramesh, N.A. Spladin, Multiferroics: progress and prospects in thin films. Nature Mater. **6**, 21 (2007)

7. C. Ganeshraj, R.N. Mahato, D. Divyaa, P.N. Santhosh, Magnetic, electrical transport and structural investigations of orthorhombic perovskite Pr_2MnFeO_6. J. Appl. Phys. **107**, 09E305 (2010)

8. R. Tholkappiyan, L.M. Azarudeen, G. Anandkumar, K. Vishista, "Characterization of Sm doped CaO phosphor prepared by co-precipitation method", advanced science. Eng Med **8**, 57 (2016)

9. N. Das, S. Singh, A.G. Joshi, M. Thirumal, V.R. Reddy, L.C. Gupta, A.K. Ganguli, Pr_2FeCrO_6: A Type I multiferroic. Inorg. Chem. **56**, 12712 (2017)

10. G.R. Haripriya, H.S. Nair, R. Pradheesh, S. Rayaprol, V. Siruguri, D. Singh, R. Venkatesh, V. Ganesan, K. Sethupathi, V. Sankaranarayanan, Spin reorientation and disordered rare earth magnetism in Ho_2FeCoO_6. J. Phys. Condens. Matter. **29**, 475804 (2017)

11. S. Chakraverty, A. Ohtomo, D. Okuyama, M. Saito, M. Okude, R. Kumai, T. Arima, Y. Tokura, S. Tsukimoto, Y. Ikuhara, M. Kawasaki, Ferrimagnetism and spontaneous ordering of transition metals in double perovskite La_2CrFeO_6 films. Phys. Rev. B **84**, 064436 (2011)

12. A. Pal, V.K. Prajyoti Singh, S.G. Gangwar, P. Prakash, S.K. Saha, A. Das, A.K. Manoranjan Kumar, Ghosh, and Sandip Chatterjee, B-site disorder driven multiple-magnetic phases: griffiths phase, re-entrant cluster glass, and exchange bias in Pr2CoFeO6. Appl. Phys. Lett. **114**, 252403 (2019)

13. Lu. Nianduan, X. Song, J. Zhang, Crystal structure and magnetic properties of ultrafine nanocrystalline $SmCo_3$ compound. Nanotechnology **21**, 115708 (2010)

14. X. Song, N. Lu, M. Seyring, M. Rettenmayr, W. Xu, Z. Zhang, J. Zhang, Abnormal crystal structure stability of nanocrystalline Sm_2Co_{17} permanent magnet. Appl. Phys. Lett. **94**, 023102 (2009)

15. E.E. Ateia, M.M. Arman, E. Badawy, Role of coupling divalent cations on the physical properties of SmFeO3 prepared by citrate auto combustion technique. Appl. Phys. A. **125**, 499 (2019)

16. S. Cao, H. Zhao, B. Kang, J. Zhang, W. Ren, Temperature induced spin switching in SmFeO3 single crystal. Sci. Rep. **4**, 5960 (2014)

17. Z. Dong, S. Yin, Structural, magnetic and magnetocaloric properties in perovskite RE_2FeCoO_6 (RE = Er and Gd) compounds. Ceram. Int. **46**, 1099–1103 (2020)

18. M. Das, P. Mandal, Nonlinear magnetodielectric and magnetocaloric properties of double perovskite Ho_2FeCoO_6. Physica B **571**, 32–35 (2019)

19. G.R. Haripriya, R. Pradheesh, M.N. Singh, A.K. Sinha, K. Sethupathi, V. Sankaranarayanan, Temperature dependent structural studies on the spin correlated system $A_2FeCoO6$ (A= Sm, Eu, Dy and Ho) using synchrotron radiation. AIP. Adv. **7**, 055826 (2017)

20. G.R. Haripriya, R. Pradheesh, K. Sethupathi, V. Sankaranarayanan, The order of magnetic phase transitions in disordered double perovskite oxides Sm_2FeCoO_6 and Dy2FeCoO6. AIP. Adv. **8**, 101340 (2018)

21. A. Pal, S. Ghosh, A.G. Joshi, S. Kumar, S. Patil, P.K. Gupta, P. Singh, V.K. Gangwar, P. Prakash, R.K. Singh, E.F. Schwier, M. Sawada, K. Shimada, A.K. Ghosh, A. Das, S. Chatterjee, Investigation of multi-mode spin-phonon coupling and local B-site disorder in Pr_2CoFeO_6 by Raman spectroscopy and correlation with its electronic structure by XPS and XAS studies. J. Phys. Condens. Matter. **31**, 275802 (2019)

22. R. Pradheesh, H.S. Nair, V. Sankaranarayanan, K. Sethupathi, Exchange bias and memory effect in double perovskite Sr2Fe-CoO6. Appl. Phys. Lett. **101**, 142401 (2012)

23. H.M. Rietveld, A profile refinement method for nuclear and magnetic structures. J. Appl. Crystallogr. **2**, 65–71 (1969)

24. K. Momma, F. Izumi, VESTA 3 for three-dimensional visualization of crystal, volumetric and morphology data. J. Appl. Crystallogr. **44**, 1272–1276 (2011)

25. M.W. Lufaso, P.W. Barnes, P.M. Woodward, Structure prediction of ordered and disordered multiple octahedral cation perovskites using SPuDS. Acta Cryst. B **62**, 397 (2006)

26. N. Pradhani, P.K. Mahapatra, R.N.P. Choudhary, Effect of cerium oxide addition on optical, electrical and dielectric characteristics of $(Bi_{0.5}Na_{0.5})TiO_3$ ceramics. J. Phys. Mater. **1**, 015007 (2018)

27. V. Purohit, R. Padhee, R.N.P. Choudhary, Dielectric and impedance spectroscopy of $Bi(Ca_{0.5}Ti_{0.5})O_3$ ceramic. Ceram. Int. **44**, 3993 (2018)

28. Y. Zheng, W. Zhuang, X. Xing, J. Zhong, R. Liu, Y. Li, Y. Liu, Y. Hu, Synthesis, structure and luminescent properties of a new blue-green-emitting garnet phosphor $Ca_2LuScZrAl_2GeO_{12}$:Ce^3+. RSC. Adv. **6**, 68852 (2016)

29. A. Kokhanovsky, Physical interpretation and accuracy of the Kubelka–Munk theory. J. Phys. D Appl. Phys. **40**, 2210–2216 (2007)

30. M.N. Iliev, M.V. Abrashev, A.P. Litvinchuk, V.G. Hadjiev, H. Guo, A. Gupta, Raman spectroscopy of ordered double perovskite La$_2$CoMnO$_6$ thin films. Phys. Rev. B. **75**, 104118 (2007)

31. M.O. Ramirez, M. Krishnamurthi, S. Denev, A. Kumar, S.Y. Yang, Y.H. Chu, E. Saiz, J. Seidel, A.P. Pyatakov, A. Bush, D. Viehland, J. Orenstein, R. Ramesh, V. Gopalan, Two-phonon coupling to the antiferromagnetic phase transition in multiferroic BiFeO3. Appl. Phys. Lett. **92**, 022511 (2008)

32. M.K. Singh, S. Ryu, H.M. Jang, Polarized Raman scattering of multiferroic BiFeO$_3$ thin films with pseudo-tetragonal symmetry. Phys. Rev. B **72**, 132101 (2005)

33. M.P. Singh, K.D. Truong, S. Jand, P. Fournier, Magnetodielectric effect in double perovskite La$_2$CoMnO$_6$ thin films. J. App. Phys. **107**, 09D917 (2010)

34. R.D. Mero, K. Ogawa, S. Yamada, H.L. Liu, Optical study of the electronic structure and lattice dynamics of NdBaMn$_2$O$_6$ single crystals. Sci. Rep. **9**, 18164 (2019)

35. J. Anthoniappen, W.S. Chang, F.M. Ruiz, C.S. Tu, C.T. Blaise, P.Y. Chen, C.S. Chen, H. Manaay, J. Alloys. Compd. **790**, 587–596 (2019)

36. M.C. Weber, M. Guennou, H.J. Zhao, J. Iniguez, R. Vilarinho, A. Almeida, J.A. Moreira, J. Kreisel, Raman spectroscopy of rare-earth orthoferrites *R*FeO$_3$ (*R*=La, Sm, Eu, Gd, Tb, Dy). Phys. Rev. B **94**, 214103 (2016)

37. H. Guo, J. Burgess, S. Street, A. Gupta, T.G. Calvarese, M.A. Subramanian, Structural and magnetic properties of epitaxial thin films of the ordered double perovskite La2CoMnO6. App. Phys. Lett. **89**, 022509 (2006)

38. P. Chandramohan, M.P. Srinivasan, S. Velmurugan, S.V. Narasimhan, Cation distribution and particle size effect on Raman spectrum of CoFe$_2$O$_4$. J. Solid State Chem. **184**, 89–96 (2011)

39. M.N. Iliev, M.V. Abrashev, H.-G. Lee, V.N. Popov, Y.Y. Sun, C. Thomsen, R.L. Meng, C.W. Chu, Raman spectroscopy of orthorhombic perovskite like YMnO$_3$ and LaMnO$_3$. Phys. Rev. B **57**, 2872–2877 (1998)

40. G. Santosh Babu, V. Subramanian, V.R.K. Murthy, R.L. Moreira, R.P.S.M. Lobo, Crystal structure, Raman spectroscopy, far-infrared, and microwave dielectric properties of (1–x)La(MgSn)$_{0.5}$O$_3$-xNd(MgSn)$_{0.5}$O$_3$ system. J. Appl. Phys. **103**, 084104 (2008)

41. A. Naveen Kumar, D.M. Jnaneshwara, H. Nagabhushana, C. Pratapkumar, C.R. Ravikumar, M.R. Anil Kumar, T.R. Shashi Shekhar, S.C. Prashantha, Photoluminescence, photocatalytic and electrochemical performance of La10Si6O27: Sm3+ nanophosphor: It's applications in display, photocatalytic and electrochemical sensor. Appl. Surf. Sci. Adv. **4**, 100070 (2021)

42. M. Shoaib, G. Rooh, R. Rajramakrishna, N. Chanthima, H.J. Kim, S. Tuscharoen, J. Kaewkhao, Physical and luminescence properties of samarium doped oxide and oxyfluoride phosphate glasses. Mater. Chem. Phys. **229**, 514–522 (2019)

43. B. Lei, Y. Liu, G. Tang, Spectra and long-lasting properties of Sm^{3+} doped yttrium oxysulfide phosphor. Mater. Chem. Phys. **87**, 227–232 (2004)

44. T. Izumitani, S.A. Payne, luminescence of Sm^{3+} doped fluoride glasses. J. lumen. **54**, 337–344 (1993)

45. Hu. Lanying, H. Song, G. Pan, B. Yan, R. Qin, Q. Dai, L. Fan, S. Li, X. Bai, Photoluminescence properties of samarium doped TiO$_2$ semiconductor nanocrystalline powders. J. lumen. **127**, 371–376 (2007)

46. J. Xiang, M. Yang, Yi. Che, J. Zhu, Y. Mao, K. Xiong, H. Zhao, Photoluminescence investigation of novel reddish-orange phosphor Li2NaBP2O8:sm3+ with high CP and low CCT. Ceram. Int. **45**, 7018–7024 (2019)

47. U.B. Gokhe, K.A. Koparkar, S.K. Omanwar, Synthesis and photoluminescence properties of near-UV pumped novel Sm^{3+}doped β-LiAlSiO$_4$ phosphor for red-orange LEDs. J. Alloy. Compd. **689**, 992–997 (2016)

48. K. Bhargavi, M. SrinivasaReddy, P. RaghavaRao, N. Narasimha Rao, M. SundaraRao, V. RaviKumar, N. Veeraiah, The structural influence of aluminium ions on emission characteristics of Sm^{3+} ions in lead aluminium silicate glass system. Mater. Res. Bull. **47**, 267–273 (2012)

49. R.B. Basavaraj, H. Nagabhushana, B.D. Prasad, S.C. Sharma, S.C. Prashantha, B.M. Nagabhushana, A single host white light emitting Zn2SiO4: Re3+ (Eu, Dy, Sm) phosphor for LED applications. Optik-Int. J. Light. Electron. Opt. **126**, 1745–1756 (2015)

50. T. Katayama, A. Chikamatsu, Y. Hirose, M. Minohara, H. Kumigashira, I. Harayama, D. Sekiba, T. Hasegawa, Ferromagnetism with strong magnetocrystalline anisotropy in A-site ordered perovskite YBaCo$_2$O$_6$ epitaxial thin film prepared via wet-chemical topotactic oxidation. J. Mater. Chem. C **6**, 3445–3450 (2018)

51. Y. Shimakawa, M. Azuma, N. Ichikawa, Multiferroic compounds with double perovskite structures. Materials **4**, 153–168 (2011)

52. M.M. Seikh, V. Pralong, O.I. Lebedev, V. Caignaert, B. Raveau, The ordered double perovskite PrBaCo$_2$O$_6$: synthesis, structure, and magnetism. J. Appl. Phys. **114**, 013902 (2013)

53. V.G. Chilkuri, N. Suaud, N. Guihery, High-Spin chains and crowns from double-exchange mechanism. Curr. Comput-Aided. Drug. Des. **6**, 39 (2016)

54. R. Pradheesh, H.S. Nair, C.M.N. Kumar, J. Lamsal, R. Nirmala, P.N. Santhosh, W.B. Yelon, S.K. Malik, V. Sankaranarayanan, K. Sethupathi, Observation of spin glass state in weakly ferromagnetic Sr$_2$FeCoO$_6$ double perovskite. J. Appl. Phys. **111**, 053905 (2012)

55. S.B. Hammouda, F. Zhao, Z. Safaei, D.L. Ramasamy, B. Doshi, M. Sillanpaa, Sulfate radical-mediated degradation and mineralization of bisphenol F in neutral medium by the novel magnetic Sr$_2$CoFeO$_6$ double perovskite oxide catalyzed peroxymonosulfate: influence of co-existing chemicals and UV irradiation. Appl. Catal. B. Environ. **233**, 99–111 (2018)

56. F. Fauth, E. Suard, V. Caignaert, Intermediate spin state of Co^{3+} and Co^{4+} ions in La$_{0.5}$Ba$_{0.5}$CoO$_3$ evidenced by Jahn-Teller distortions. Phys. Rev. B **65**, 060401 (2001)

57. T. Nakajima, M. Ichihara, Y. Ueda, New A-site Ordered perovskite cobaltite LaBaCo$_2$O$_6$: synthesis, structure, physical property and cation order-disorder effect. J. Phys. Soc. Jpn. **74**, 1572–1577 (2005)